SURFACE AND INTERFACE ANALYSIS
Surf. Interface Anal. 2004; **36**: 1367–1372
Published online in Wiley InterScience (www.interscience.wiley.com). DOI: 10.1002/sia.1923

SIA

Use of C_{60} cluster projectiles for sputter depth profiling of polycrystalline metals

S. Sun,[1] C. Szakal,[1] T. Roll,[2] P. Mazarov,[2] A. Wucher[2] and N. Winograd[1]*

[1] Department of Chemistry, Pennsylvania State University, 184 Materials Research Institute Building, University Park, PA 16802, USA
[2] Physics Department, University of Duisburg-Essen, 45117 Essen, Germany

Received 30 March 2004; Revised 11 May 2004; Accepted 12 May 2004

We have investigated the merits of fullerene cluster ions as projectiles in time-of-flight secondary neutral mass spectrometry (ToF-SNMS) sputter depth profiling of an Ni : Cr multilayer sample similar to the corresponding NIST depth profiling standard. It is shown that sputter erosion under bombardment with C_{60}^+ ions of kinetic energies between 10 and 20 keV provides good depth resolution corresponding to interface widths of several nanometres. This depth resolution is maintained during the complete removal of the multilayer stack with a total thickness of 500 nm. This finding is in contrast to the case where atomic Ga^+ projectile ions of comparable kinetic energy are used, demonstrating the unique features of cluster projectiles in sputter depth profiling. Copyright © 2004 John Wiley & Sons, Ltd.

INTRODUCTION

Sputter depth profiling has proved to be a powerful technique to determine the chemical composition of a solid in the near-surface region. However, there are a number of well-documented problems associated with the technique, such as beam-induced interlayer mixing and the loss of depth resolution with increasing eroded depth. In particular, the latter effect is often caused by the development of topographic roughness during sputter removal of material from the surface.

One approach to help resolve the problems is to employ low-energy primary ion bombardment.[1,2] This approach, however, has its disadvantages because it is difficult to focus the beam to a small size of micrometres or less, and the sputter yields decrease significantly for primary ions with low kinetic energies. Another approach is to use polyatomic or cluster projectiles such as CF_3, $^3N_2O^4$ or SF_5.[5,6]

Because the polyatomic or cluster ions dissociate upon collision with the target surface, the initial ion energy is split among the constituent atoms. As a consequence, there is a shallow penetration of incident particles and the deposited energy remains close to the surface. These phenomena reduce interlayer mixing and yield higher depth resolution than atomic projectiles with the same kinetic energy. Also, Gillen and co-workers[6] demonstrated that SF_5^+ causes less topographic roughness in the eroded crater. The build-up of topography is a major reason for the degradation of depth resolution. Similar trends have been found by Yamada and co-workers,[7] who demonstrated that ion bombardment using rare gas clusters may produce much smoother surfaces than bombardment with atomic projectiles.

*Correspondence to: N. Winograd, Department of Chemistry, Pennsylvania State University, 184 Materials Research Institute Building, University Park, PA 16802, USA. E-mail: nxw@psu.edu
Contract/grant sponsor: National Science Foundation.

A specific example of a thin-film system where the achievable depth resolution is determined by sputter erosion-induced topography is a multilayer stack of alternating Ni and Cr metallization layers on an Si substrate. In fact, this system has been a test case for sputter depth profiling and thus is available as a NIST standard reference material (SRM 2135a). Owing to the polycrystalline nature of the individual metal layers, surface roughness builds up during ion beam erosion due to varying erosion rates between different grains. This variation is generated by the dependence of the total sputtering yield on the crystallographic orientation of the grain surface. As a consequence, the depth resolution determined from the apparent transition width measured at the interfaces between the different layers generally degrades with increasing eroded depth.

Numerous studies have addressed the depth resolution that can be achieved in sputter depth profile analysis of Ni : Cr multilayers and its dependence on ion bombardment parameters such as mass, kinetic energy and impact angle of the projectile ions.[8] Various surface analytical techniques such as secondary ion (neutral) mass spectrometry (SIMS or SNMS),[9] Auger electron spectroscopy (AES)[10] and x-ray photoelectron spectroscopy (XPS)[11] have been employed to characterize the actual surface exposed during continued ion bombardment. It has been shown that a depth resolution of the order of several nanometres can be achieved and maintained throughout several 100 nm of eroded depth if low-energy ions are used under non-normal incidence conditions. By rotating the sample during the ion bombardment, Zalar[12] managed to maintain a depth resolution of $\sim$3 nm throughout the entire layer stack.

Cluster beam projectiles such as SF_5^+ have been explored recently for sputter depth profile analysis of various systems, including Ni : Cr multilayer samples.[6] To carry this work further, we have reported recently[13] on the use of a Buckminsterfullerene ion source[14] for depth profiling of such a sample. Using a primary 15 keV C_{60}^+ ion beam,

Copyright © 2004 John Wiley & Sons, Ltd.

we can resolve all individual layers with a depth resolution of several nanometres throughout a 500 nm erosion depth. In this paper we expand on these initial observations and investigate the sensitivity of the depth profiles measured on the same Ni : Cr multilayer to the impact energy of the fullerene clusters. In order to examine the role of ion beam-induced topography formation, the bottom of the eroded crater is investigated by atomic force microscopy (AFM) after acquisition of the depth profile. The results demonstrate that even at the highest impact energy employed a depth resolution of several nanometres is easily obtained and maintained throughout removal of the complete multilayer stack. This finding is of extreme importance with respect to high-resolution three-dimensional surface and thin-film analysis applications, because the high kinetic impact energy permits tight focusing of the primary ion beam and hence good lateral resolution.

EXPERIMENTAL

The experiments were performed using a time-of-flight (ToF) SIMS spectrometer that has been described in great detail previously.[15] The system has been modified recently to accommodate both a liquid-metal Ga^+ ion source and a newly developed fullerene ion source.[14] Both ion beams impinge onto the investigated surface under an impact angle of 40° with respect to the surface normal. The fullerene ions are produced by electron impact ionization of C_{60} vapour. The source generally produces singly and doubly charged C_{60} ions, the flux ratio of which depends on the electron impact energy. In our current experiments, an electron energy of 30 eV was used, which is appropriate to produce only singly charged C_{60}^+ ions.[13]

The Ni : Cr multilayer sample consists of nine alternating layers of Cr and Ni on an Si(100) substrate with nominal layer widths of 53 and 66 nm, respectively. The sample was rinsed with hexane and methanol and then dried with nitrogen gas. Depth profiling was performed by alternating sputter erosion cycles and data acquisition cycles. During the erosion cycles, either the C_{60}^+ or the Ga^+ ion beam was operated in d.c. mode and rastered across an area of $400 \times 400\ \mu m^2$. In a data acquisition cycle, static time-of-flight ToF-SIMS spectra of the currently exposed surface are measured with the same ion source now operating in pulsed mode and rastered across a central crater area of $50 \times 50\ \mu m^2$ to minimize disturbances arising from the crater edges. The C_{60}^+ source was operated at beam energies of 10, 15 and 20 keV, with the resulting beam currents being around 0.2, 0.6 and 0.8 nA, respectively. Prior to the acquisition of each depth profile, it was made sure that the ion beam was focused to a diameter of ~30 μm (FWHM) as determined from line scans across ion-induced electron emission images obtained on SEM grids. In order to convert sputter time into projectile ion fluence, the selected raster area was corrected for the appropriate beam diameter. This was not necessary for the 15 keV Ga^+ beam with a diameter of ~1 μm and a total current of ~1 nA.

In order to avoid the matrix effect typically encountered in SIMS and to enhance the measured signal intensity, the experiments were performed in the SNMS mode of the instrument where neutral particles released from the ion-bombarded surface are post-ionized by a pulsed laser and then detected by the ToF spectrometer. The timing of the experiment was arranged such that the sample is kept at ground potential during the primary ion pulse of 1000 ns length. This relatively long pulse duration is chosen to ensure that particles of all emission velocities are present in the post-ionization volume at the time the ionization laser fires. About 100 ns after the end of the primary ion pulse, the sample stage is switched to high positive potential, thus generating an extraction field that sweeps secondary ions present in the post-ionization volume into the ToF spectrometer. The ionization laser is fired after another delay of ~100 ns. This additional laser delay is introduced in order to separate secondary ion and post-ionized neutral peaks in the ToF spectrum. Because the start time for secondary ions and post-ionized neutrals is determined by the extraction and laser firing times, respectively, the secondary ion peaks appear earlier (by a time equivalent to the laser delay) than those of the corresponding post-ionized neutrals.

The 800 nm laser pulses are produced by a Ti : sapphire femtosecond laser system described in detail earlier.[16] Briefly, an Ar^+ ion laser is used to pump the Ti : sapphire oscillator and produce 800 nm laser pulses with 50 fs pulse widths and ~300 nJ per pulse energy. The output pulses are then amplified to reach 2.3 mJ per pulse at a 1 kHz repetition rate. The laser beam is coupled into the mass spectrometer in a direction parallel to and ~1 mm above the sample surface using a CaF_2 lens with 25 cm focal length. In order to achieve a beam diameter of ~200 μm in the ionization region above the surface, the lens is retracted from the focal position by ~12.5 mm along the optical axis, thus producing a peak power density of $2.2 \times 10^{13}\ W\ cm^{-2}$ within the ionization volume.

After completion of the depth profile analysis, the eroded crater was investigated by AFM to study the roughness that had been generated at the crater bottom during the ion erosion process. After removing the samples from the ultrahigh vacuum system, AFM images were acquired at atmospheric pressure using a digital instrument atomic force microscope (Digital Instrument Dimension 3100) in tapping mode at 1 Hz.

RESULTS AND DISCUSSION

In order to investigate the effect of the type and energy of the primary ion projectiles on the depth resolution, the Ni : Cr depth profiles were measured with C_{60}^+ for 20, 15 and 10 keV kinetic energies and compared with a depth profile taken with Ga^+ at 15 keV kinetic energy. Time-of-flight SNMS mass spectra that have been acquired at the interface region between the first Cr layer and the second Ni layer with 20 keV C_{60}^+ and 15 keV Ga^+ bombardment are depicted in Fig. 1. The peak occurring at an apparent fractional mass of 51.5 Da corresponds to $^{52}Cr^+$ secondary ions that have been intentionally displaced towards smaller flight times (see previous section). The fact that the flight time peaks in both spectra appear slightly different arises from small differences in the relative timing of primary

Copyright © 2004 John Wiley & Sons, Ltd.

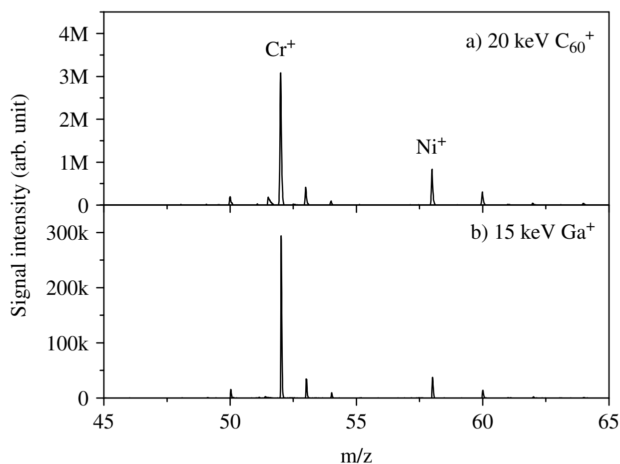

Figure 1. Time-of-flight mass spectra of post-ionized neutral particles measured at the interface between the first Cr and the second Ni layer of an Ni : Cr multilayer stack. The sample was bombarded with 20 keV $C_{60}{}^{+}$ (a) and 15 keV Ga^{+} (b) ions for sputter erosion and data acquisition. Post-ionization laser: 800 nm, 2.2×10^{13} W cm^{-2}.

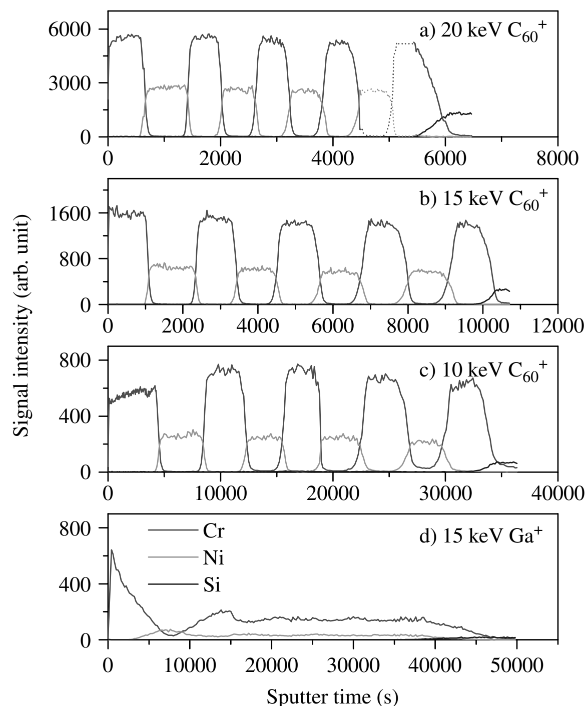

Figure 2. Integrated signals of post-ionized neutral atoms vs. total sputter erosion time under bombardment with: (a) 20 keV $C_{60}{}^{+}$ (data not recorded over the region identified by the dashed line); (b) 15 keV $C_{60}{}^{+}$; (c) 10 keV $C_{60}{}^{+}$; (d) 15 keV Ga^{+}. Post-ionization laser: 800 nm, 2.2×10^{13} W cm^{-2}.

ion and laser pulses. These variations are induced by slightly different impact times of $C_{60}{}^{+}$ and Ga^{+} primary ions.

Because the data have been recorded in direct charge digitization mode, where one measured flight time peak may consist of many detected ions, the vertical scale in Fig. 1 is given in arbitrary units that refer to the amplified signal recorded by the transient digitizer. The scale is, however, the same for both displayed spectra. It is seen that the $C_{60}{}^{+}$ projectiles produce about a tenfold increase in the measured signal as compared with Ga^{+}. Because we are detecting the sputtered neutral species, we attribute that finding to a corresponding increase of the respective sputtering yields, an assessment that is in agreement with our previous observations and corresponding molecular dynamics computer simulations.[17]

The raw depth profile data, i.e. the integrated signal of post-ionized neutral ^{58}Ni and ^{52}Cr atoms as a function of the total ion bombardment time accumulated over subsequent sputter erosion cycles, are shown in Fig. 2. The data have been plotted for 20, 15, and 10 keV $C_{60}{}^{+}$ and 15 keV Ga^{+}. In all cases, data acquisition has been performed using the same projectile and impact energy as used during sputter erosion. It is seen that at all investigated impact energies the cluster ion erosion clearly allows resolution of all individual layers. Moreover, the apparent depth resolution is maintained without significant degradation throughout removal of the complete multilayer stack, with a total thickness of ~530 nm. These findings are in pronounced contrast to the atomic ion erosion where only the first layer is resolved. From these observations, we conclude that C_{60} cluster bombardment offers great improvement over atomic ion bombardment and represents a very efficient tool for sputter depth profile analysis of samples such as the one investigated here.

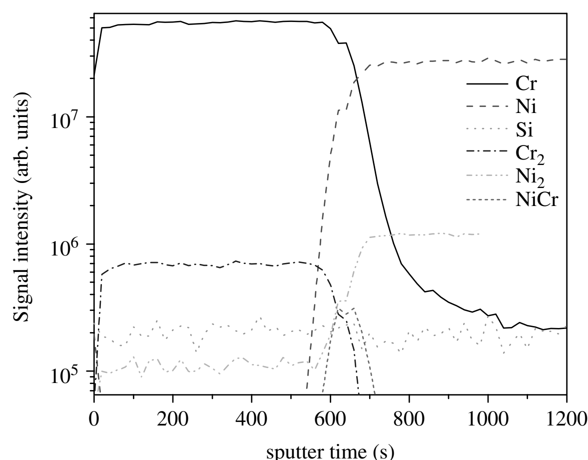

Figure 3. Integrated signals of post-ionized neutral atoms and diatomic molecules vs. total sputter erosion time for the profile shown in Fig. 1(a).

Besides the atomic signals depicted in Fig. 2, the measured ToF spectra contain peaks of molecular species composed of more than one sample atom. In order to illustrate the relative importance of such signals, the integrated peaks of the most abundant diatomic molecules Cr_2, Ni_2 and NiCr during removal of the first two layers are displayed in Fig. 3. First, it is seen that the molecular signals are negligibly small in all cases compared with the atomic signals. Moreover, although homonuclear molecules follow the same qualitative variation as that of the corresponding atoms, the heteronuclear molecule NiCr exhibits the expected behaviour with a

Copyright © 2004 John Wiley & Sons, Ltd.

maximum at the interface between the Cr and the Ni layer. The Ni_2 signal exhibits a non-negligible background due to a small Cr_2O interference in the Cr layer and therefore appears to rise less steeply at the interface than the Ni signal itself.

As can be observed from the C_{60} depth profiles, the signal intensity obtained for Ni atoms in an Ni layer is ~1.8-fold lower than that of Cr atoms obtained in a pure Cr layer. This finding can be attributed to two possible reasons: the Ni layer may exhibit a lower sputtering yield than the Cr layer; or the Ni atoms have a lower post-ionization probability than Cr atoms (or a combination of both). In order to determine what the cause is, we calculate the total sputtering yield of Ni and Cr layers from the known layer thickness and the ion fluence needed to profile across an individual layer at different kinetic energies. Using the known raster size employed during the sputter cycles (corrected for the ion beam diameter), we obtain the sputtering yield values tabulated in Table 1. The results show that in all cases the sputtering yield of Ni is slightly higher than that of Cr, the difference increasing with decreasing impact energy. This finding is in accord with the fact that Ni and Cr have about equal masses and sublimation energies. Note that the sputtering yield induced by C_{60}^+ is about one order of magnitude higher than that from Ga^+, which agrees with similar results obtained on polycrystalline Ag surfaces.[18] With the raster size and primary ion currents employed here, the erosion rates achieved are ~5 nm min^{-1} for 20 keV C_{60}^+ and 0.4 nm min^{-1} for 15 keV Ga^+. By shrinking the raster size to dimensions comparable to the employed C_{60}^+ beam diameter, it is possible in principle to increase the corresponding erosion rate to values of ~900 nm min^{-1} while still being able to perform a meaningful analysis with the beam centred in the eroded crater.

Because the sputtering yields for Ni are apparently larger than those for Cr, the measured signal intensity difference must result from differences in post-ionization probabilities for Ni and Cr atoms. More quantitatively, the measured signal is described by[19]

$$S(X) = I_p Y_{\text{tot}} D_X c_X \tag{1}$$

where I_p denotes the primary ion current, Y_{tot} is the total sputtering yield, D_X is a factor containing the post-ionization probability as well as the collection efficiency of sputtered neutral particles and c_X denotes the concentration of element X (Cr, Ni or Si) at the surface. Correcting for the sputtering yield ratio taken from Table 1, we can determine a relative sensitivity factor $R_{\text{Ni}} = D_{\text{Ni}}/D_{\text{Cr}}$ from the measured signal ratio in the Ni and the Cr layer, respectively. Similarly, R_{Si} is determined from the signal measured in the Si substrate. With the assumption that the sample contains only Cr, Ni and Si and molecular signals are negligible (cf. Fig. 2), application of Eqn. (1) leads to the well-known SNMS quantitation

$$c_X = \frac{S_X/R_X}{S_{\text{Cr}} + S_{\text{Ni}}/R_{\text{Ni}} + S_{\text{Si}}/R_{\text{Si}}} \tag{2}$$

where x refers to Cr, Ni or Si, respectively.

Table 1. Total sputtering yield measured in individual Ni and Cr layers, respectively, under bombardment with C_{60}^+ projectiles at different kinetic impact energies

	C_{60}^+			Ga^+
Layer	10 keV	15 keV	20 keV	15 keV
Ni	197	190	237	14.8
Cr	140	165	216	14.2

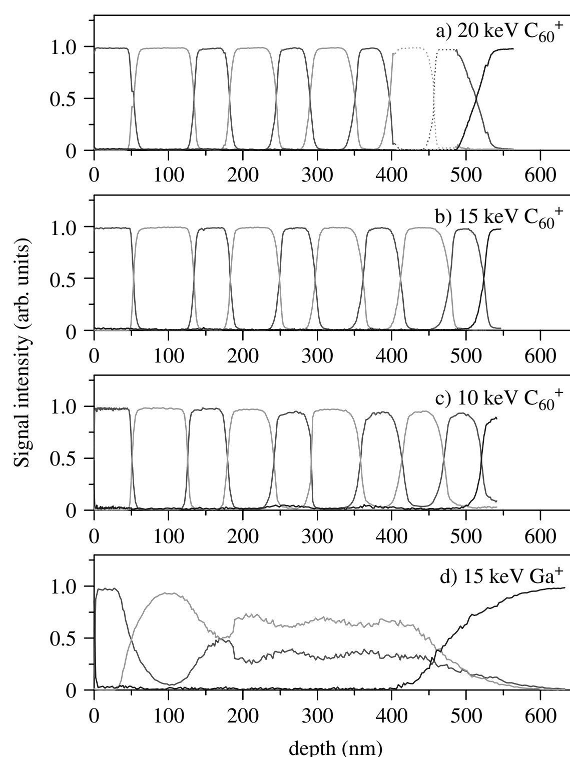

Figure 4. The Ni : Cr depth profiles, i.e. surface concentration vs. depth, under bombardment with: (a) 20 keV C_{60}^+ (data not recorded over the region identified by the dashed line); (b) 15 keV C_{60}^+; (c) 10 keV C_{60}^+; (d) 15 keV Ga^+. Evaluated from the measured data using the methods described in the text.

In order to calibrate the depth scale, it is necessary to determine possible variations of the total sputtering yield Y_{tot} as a function of sputter erosion time. Again applying Eq. (1), one obtains

$$Y_{\text{tot}} \propto S_{\text{Cr}} + S_{\text{Ni}}/R_{\text{Ni}} + S_{\text{Si}}/R_{\text{Si}} \tag{3}$$

Because the erosion rate is directly proportional to Y_{tot}, the weighted signal sum of Eqn. (3) allows a non-linear conversion of sputter time into eroded depth provided that the depth corresponding to one particular time is known. In the present case, we take the nominal total width of the complete multilayer stack as 529 nm and assume depth to be eroded at the point were $c_{\text{Cr}} = c_{\text{Si}} = 0.5$. The resulting calibrated depth profiles are shown in Fig. 4. It is seen that the first Ni layer appears thicker than the remaining four layers. This finding is reproduced in all C_{60}^+ depth profiles and

Copyright © 2004 John Wiley & Sons, Ltd.

therefore probably reflects a true feature of the investigated sample.

The depth resolution is determined from the apparent interface width, i.e. the depth interval between the two points where the Cr concentration in the calibrated profiles of Fig. 4 reaches values of 84% and 16%, respectively. The depth resolution obtained at the first interface is 8.7 nm for 20 keV C_{60}^+ bombardment and improves to 5.9 and 5.3 nm when the kinetic energy is decreased to 15 and 10 keV, respectively. The dependence of the observed interface width on the total eroded depth is illustrated in Fig. 5. Although there is a slight degradation of depth resolution with increasing depth, its magnitude is much less dramatic than for atomic projectiles (represented by the Ga^+ data in Fig. 4(d)). For cluster beam depth profiling, the common argument is that the projectiles will dissociate upon collision with the target molecules and the initial kinetic energy will be split between each constituent atom of the impinging cluster. In one sense, this resembles the use of ultra-low-energy atomic primary ion projectiles, which are known to minimize interlayer mixing effects and thereby provide improved depth resolution.[19,20] Applying this concept to C_{60} projectiles, the kinetic energy per constituent carbon atom is 333, 250 and 167 eV for the three total impact energy values employed here. From this perspective, it appears understandable that the interface widths reported here are comparable to those typically measured with atomic projectiles of much lower kinetic energy.[9]

In order to determine the ion beam-induced topography, AFM images were taken to examine the crater bottom at the end of the depth profiles displayed in Fig. 4. The most interesting observation is that the topography induced by the cluster projectile impact is much less pronounced than that generated by the atomic projectiles. Examples of the corresponding AFM images obtained for 20 keV C_{60}^+ and 15 keV Ga^+ bombardment are displayed in Fig. 6. Evaluating the image data, we observe that the roughness determined after prolonged 20 keV C_{60}^+ impact is 8 nm (rms).

In contrast, Ga^+ projectiles are found to produce a much more pronounced topography. To illustrate this effect, the roughness evaluated from AFM images taken at different depths eroded by 15-keV Ga^+ bombardment is depicted in Fig. 7. It is seen that the roughness increases linearly with increasing depth, as is expected if the topography is caused by lateral sputtering yield variations. This observation supports the notion that the large degradation of depth resolution observed for Ga^+ projectiles is mostly arising from ion bombardment-induced surface topography.

At zero depth, an intrinsic roughness of ~7 nm (rms) is found in Fig. 7. It is of note that this value is practically identical to that determined with 20 keV C_{60}^+ bombardment after erosion of the complete Ni : Cr layer stack. Apparently, the bombardment-induced roughening effect is virtually absent for cluster projectiles, indicating that the crystallite

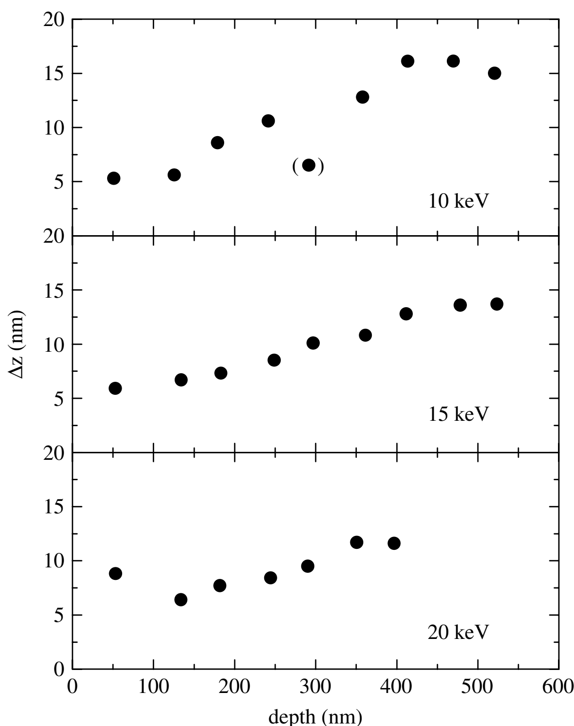

Figure 5. Apparent 84%-16% interface width as a function of sputtered depth for C_{60}^+ ion bombardment of different kinetic impact energy.

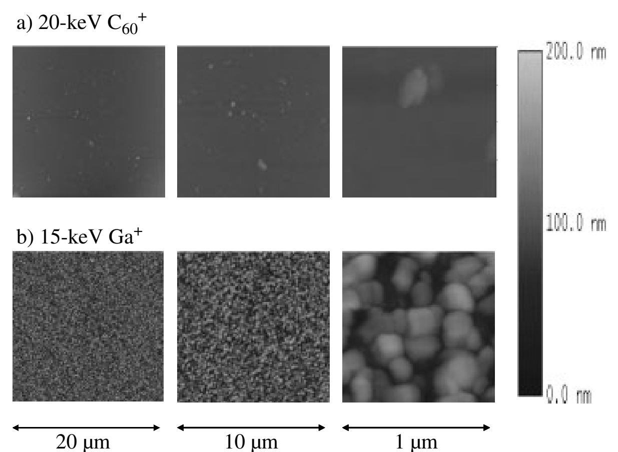

Figure 6. Atomic force microscopy images of the crater bottom after completion of the depth profile analysis using 20 keV C_{60}^+ (a) and 15 keV Ga^+ (b) primary ions.

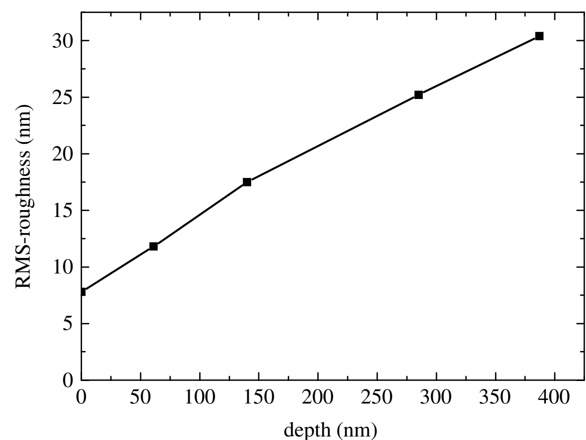

Figure 7. The rms roughness evaluated from AFM images of the crater bottom during sputter erosion using 15 keV Ga^+ projectiles as a function of eroded depth.

Copyright © 2004 John Wiley & Sons, Ltd.

orientation dependence of the total sputtering yield is in this case much less pronounced than under atomic projectile bombardment. This observation is elucidated by recent molecular dynamics computer simulations[17] comparing the sputtering processes induced by C_{60} and Ga projectiles, respectively. The simulations show that the nature of the collision cascades generated under C_{60} impact is very different from that typically observed for atomic projectiles. The visualization included in Ref. 17 reveals that a C_{60} projectile impact leads to the development of a relatively large excited volume, in which every memory of the original crystal structure is completely erased after a few tens of femtoseconds.

The simulations also show that C_{60} has shorter penetration depth and causes less interlayer mixing than Ga. On the other hand, they indicate that the average escape depth of sputtered particles is larger for C_{60} bombardment. Note that the escape depth limits the intrinsic depth resolution of the ToF-SIMS/SNMS technique, which is induced by the (static) data acquisition process and therefore is independent of eroded depth. From the simulation results,[17] one would infer that a single C_{60} impact leads to the removal of material from a crater of ~5 nm lateral diameter and ~1.8 nm depth. This finding suggests that up to seven atomic layers may contribute to the measured mass spectrometric signal, leading to an intrinsic depth resolution of the order of 2 nm. Comparing simulations performed at different impact energies of the C_{60} projectile (details available from the author upon request) it is interesting to note that the lateral extension of the removed volume increases more strongly with increasing energy than its depth. For the impact energy range explored here, the crater depth is estimated to vary between 1.6 nm at 10 keV to 2.1 nm at 20 keV. This finding explains why we do not observe large differences in depth resolution between these impact energies.

The finding that the observed depth resolution does degrade with increasing depth, on the other hand, sheds light on microscopic processes occurring under C_{60} cluster ion bombardment. The AFM data clearly indicate that ion bombardment-induced roughness can be ruled out as the source of the degradation. Because the intrinsic depth resolution must be independent of eroded depth, we have to conclude that cumulative interlayer mixing effects must be responsible for the trends observed in Fig. 5.

CONCLUSION

The use of a C_{60}^+ primary ion source offers clear advantages over the Ga^+ source for depth profiling. It is demonstrated that C_{60}^+ projectiles of kinetic energies as high as 20 keV can be employed to resolve clearly all the individual layers of an Ni : Cr multilayer stack with several nanometres depth resolution, whereas no meaningful analysis is possible with 15 keV Ga^+ projectiles. These advantages are attributed to the higher sputtering yield, less interlayer mixing and, most importantly, the absence of ion beam-induced topography evolution resulting from C_{60}^+ bombardment. The depth resolution achieved here with a relatively high kinetic impact energy is comparable to the best values reported in the literature for this type of sample using low-energy atomic primary ion sources and sample rotation to minimize ion bombardment-induced roughness. This fact is of particular importance for three-dimensional imaging applications, where the sample composition is to be analysed with high lateral and depth resolution at the same time. Here, the high-energy C_{60}^+ beam can be much better focused than low-energy atomic ion beams, allowing in the present stage of development a lateral resolution of the order of several micrometres. From the data obtained here, even a combined dual-beam depth profile analysis seems feasible where the C_{60}^+ beam is used to sputter erode the surface, thereby minimizing the interlayer mixing and topography effects, whereas the data acquisition is performed with the Ga^+ ion beam, thus utilizing the submicron lateral resolution achievable with a liquid-metal ion source.

Acknowledgements

The authors thank Christine McGuiness for help in acquiring the AFM images. The authors also thank the National Science Foundation for financial support.

REFERENCES

1. Dowsett MG. *Appl. Surf. Sci.* 2003; **203**: 5.
2. Hofmann S. *Philos. Trans. R. Soc. London A* 2004; **362**: 55.
3. Reuter W, Scilla GJ. *Anal. Chem.* 1988; **60**: 1401.
4. Ronsheim PA, Fitzgibbon G. *J. Vac. Sci. Technol. B* 1992; **10**: 329.
5. Iltgen K, Bendel C, Benninghoven A, Niehuis E. *J. Vac. Sci. Technol. A* 1997; **15**: 460.
6. Gillen G, Walker M, Thompson P, Bennett J. *J. Vac. Sci. Technol. B* 2000; **18**: 503.
7. Yamada I, Matsuo J, Insepov Z, Akizuki M. *Nucl. Instrum. Methods B* 1995; **106**: 165.
8. Hofmann S, Zalar A, Circlin EH, Vajo JJ, Mathieu HJ, Panjan P. *Surf. Interface Anal.* 1993; **20**: 621.
9. Wucher A, Oechsner H, Novak F. *Thin Solid Films* 1989; **174**: 133.
10. Barna A, Barna PB, Zalar A. *Surf. Interface Anal.* 1988; **12**: 144.
11. Zalar A, Hofmann S. *Appl. Surf. Sci.* 1993; **68**: 361.
12. Zalar A, Hofmann S, Zabkar A. *Thin Solid Films* 1985; **131**: 149.
13. Sun S, Wucher A, Szakal C, Winograd N. *Appl. Phys. Lett.* 2004; **84**: 5177.
14. Weibel D, Wong S, Lockyer N, Blenkinsopp P, Hill R, Vickerman JC. *Anal. Chem.* 2003; **75**: 1754.
15. Braun RM, Blenkinsopp P, Mullock SJ, Corlett C, Willey KF, Vickerman JC, Winograd N. *Rapid Commun. Mass Spectrom.* 1998; **12**: 1246.
16. Willey KF, Brummel CL, Winograd N. *Chem. Phys. Lett.* 1997; **267**: 359.
17. Postawa Z, Czerwinski B, Szewczyk M, Smiley EJ, Winograd N, Garrison BJ. *Anal. Chem.* 2003; **75**: 4402.
18. Sun S, Szakal C, Smiley EJ, Wucher A, Winograd N. *Appl. Surf. Sci.* 2003; **231–232**: 64 .
19. Oechsner H. *Int. J. Mass Spectrom. Ion Proc.* 1995; **143**: 271.
20. Clegg JB. *Surf. Interface Anal.* 1987; **10**: 332.

Copyright © 2004 John Wiley & Sons, Ltd.